HHS Public Access

Author manuscript

J Biomed Mater Res A. Author manuscript; available in PMC 2022 September 02.

Published in final edited form as:

J Biomed Mater Res A. 2022 January ; 110(1): 76–91. doi:10.1002/jbm.a.37267.

Preparation of nanocrystalline cellulose multifunctional composite hydrogel and its application in heart valve tissue engineering

Nianfang Ma[a,b,1], **Daniel Y. Cheung**[a,1], **Jonathan T. Butcher**[a]

[a]Meinig School of Biomedical Engineering, Cornell University, Ithaca, NY 14850, USA

[b]Institute of Bioengineering, Guangdong Academy of Sciences; Guangdong Provincial Engineering Technology Research Center of Biomaterials, Guangzhou 510316, China

Abstract

Functional tissue engineered heart valves (TEHV) have been an elusive goal for nearly 30 years. Among the persistent challenges are the requirements for engineered valve leaflets that possess nonlinear elastic tissue biomechanical properties, support quiescent fibroblast phenotype, and resist osteogenic differentiation. Nanocellulose is an attractive tunable biological material that has not been employed to this application. In this study, we fabricated a series of photocrosslinkable composite hydrogels mNCC-MeGel (mNG) by conjugating TEMPO-modified nanocrystalline cellulose (mNCC) onto the backbone of methacrylated gelatin (MeGel). Their structures were characterized by FTIR, ^{1}HNMR and uniaxial compression testing. Human adipose-derived mesenchymal stem cells (HADMSC) were encapsulated within the material and evaluated for valve interstitial cell phenotypes over 14 days culture in both normal and osteogenic media. Compared to the MeGel control group, the HADMSC encapsulated within mNG showed decreased alpha smooth muscle actin (αSMA) expression and increased vimentin and aggrecan expression, suggesting the material supports a quiescent fibroblastic phenotype. Under osteogenic media conditions, HADMSC within mNG hydrogels showed lower expression of osteogenic genes, including Runx2 and osteocalcin, indicating resistance towards calcification. As a proof of principle, the mNG hydrogel, combined with a viscosity enhancing agent, was used to 3D bioprint a tall, self-standing tubular structure that sustained cell viability. Together, these results identify mNG as an attractive biomaterial for TEHV applications.

Keywords

Nonlinear biomechanics; hydrogel; methacrylated gelatin (MeGel); fibroblastic phenotype; calcification; 3D Bioprinting

Address for correspondence: Jonathan T. Butcher, PhD, 304 Weill Hall, Cornell University, Ithaca NY, 14850, Tel: 607-255-3575, Fax: 607-255-7330, jtb47@cornell.edu.

[1]Both authors contributted equally.

INTRODUCTION

Calcific heart valve disease (CAVD) affects predominately elderly and pediatric patients in developed and developing countries, respectively.[1],[2],[3] There are currently no therapeutic treatments available to prevent CAVD, and when the patient progresses to the end stage of CAVD characterized by leaflet calcification and severe stenosis, the only option is valve replacement.[4],[5] The most common valve replacement options are mechanical valves and bioprosthetic valves.[6],[7] However, while these options are adequate for the elderly population, they are problematic for pediatric patients due to multiple resizing surgeries caused by the lack of growth potential of the prosthetic valves.[8],[9]

Tissue engineered heart valves (TEHV) can provide an environment for which patient-derived cells can grow and remodel the scaffold to mimic the native valve architecture. Several types of materials have been used to fabricate TEHV to mimic the biomechanics of the valve, ranging from natural to synthetic polymers. Methacrylated gelatin (MeGel) is a common hydrogel biomaterial for tissue engineering,[10] as it is mechanically tunable and provides excellent cell adhesion properties. We have previously demonstrated the ability to bioprint heart valves using MeGel hydrogels.[11],[12] MeGel however does not exhibit nonlinear stiffening critical for valvular biomechanics.[13] Further, in bone tissue engineering applications, MeGel was found to enhance MSC osteogenic differentiation and ECM calcification, all properties of CAVD.[14] Therefore, hydrogels like MeGel will need additional modifications or compositing with other materials to reduce potentially embedded risks of calcification and/or leaflet retraction.[10],[14]

Nanocellulose is a polysaccharide composed of linear chains of linked glucose units that comes in a variety of forms and scales several orders of magnitude in size. Attribute to their special nano-size effects, superior mechanical properties and remarkable biological properties, nanocelluloses have attracted an increasing attention as reinforcement for polymer hydrogels.[15] In addition, it has also been reported that the size, morphology and mechanical properties of nanocelluloses have an effect on cells adhesion, proliferation, migration and chondrogenic differentiation.[16],[17] Utilizing these unique structural and biological properties, nanocellulose have been used in a variety of tissue engineering applications, including vascular grafts[18],[19], soft tissue orthopedics replacements (e.g. ligament, meniscus, cartilage, and nucleus pulposus)[20],[21],[22], and wound healing[23].

In many instances, incorporation of nanocellulose enhanced the modulus and modulated cell fate, particularly by promoting a chondrogenic phenotype.[24] Researchers investigated using a blend of nanocellulose for engineering heart valves, including compression molding pineapple leaf fiber nanocellulose in between polyurethane films[19] and mixing poly(vinyl alcohol) with bacterial cellulose.[25] Wang et al.[26] used cellulose nanofiber (CNF) as a reinforcing phase to effectively improve the mechanical properties of biomass-based hydrogel materials and proved CNF is conducive to cell migration and rapid transport of biomolecules. Although these studies showed nanocellulose enhanced mechanical properties and good biocompatibility, the hydrophilicity of the nanocellulose interface has posed a challenge to the use of nanocellulose as reinforcing agents, coupled with their tendency to aggregate, which made the efficient dispersion of nanocellulose in

most conventional polymeric materials challenging and may cause phase separation in some parts and bring internal stress concentration point to bulk material.[27] In order to solve the problems, it is necessary to improve the interface compatibility between the bulk polymer and nanocellulose. Unlike unmodified NCC which can only be physically blended, TEMPO (2,2,6,6-Tetramethylpiperidinyloxy or 2,2,6,6-Tetramethylpiperidine 1-oxyl)-modified nanocellulose can improve the carboxyl content and reaction activity on the surface of nanocellulose[28],[29], thereby link them to MeGel backbone through covalent conjugation of amino group and carboxyl group. In addition, a large number of negative charges attached on the surface of the oxidized nanocellulose could improve its dispersion and make the hydrogel more stable. On the other hand, nanocellulose reinforced hydrogel materials were not extensively studied to evaluate cell phenotype and tissue remodeling and there is still much room for improvement in mechanical strength of the hydrogel material.

Understanding these limitations of MeGel and the potential of TEMPO-modified nanocellulose, we sought to evaluate the potential of conjugating nanocellulose onto MeGel on strengthening the hydrogel mechanical properties and modulating cell fate while minimizing osteogenic potential for TEHV applications. Here, we prepared a series of photocrosslinkable hydrogels compositing by MeGel and TEMPO-modified nanocrystalline cellulose(mNCC) through blending and covalent conjugation. The structure was characterized by FTIR, ^{1}HNMR. Human adipose-derived mesenchymal stem cells (HADMSC) were encapsulated within the material and evaluated for quiescent and activated valve interstitial cell markers.

MATERIALS AND METHODS

Material synthesis

Methacrylated gelatin was synthesized as previously described.[10],[11] Briefly, 10% (w/v) porcine skin gelatin (Type A, 300 bloom, Sigma) was dissolved in ultrapure water at 40 °C, methacrylic anhydride was added at a 1:5 v/v ratio, and the reaction proceeded for one hour at 40 °C. The mixture was dialyzed (MWCO 1 kDa, Spectrum Labs) in a 40 °C water bath for one week and lyophilized. Next, varying amounts of TEMPO-modified nanocrystalline cellulose (mNCC, 6% solids, Cellulose Lab) was conjugated to 7% MeGel via NHS/EDC in 10 mL ultrapure water (Table 1). The reagent ratio are as follows and scaled linearly: 0.4% mNCC/12.5 mg NHS/25 mg EDC. The reaction proceeded at room temperature with constant shaking for at least three hours, dialyzed for five days, and lyophilized. All materials were UV sterilized for at least one hour prior to use.

^{1}HNMR

The resulting conjugated mNCC-MeGel (mNG) was verified by ^{1}HNMR and FTIR. Infrared spectra were obtained with FTIR Analyzer (Brucker Tensor 27). FTIR-ATR measurements were carried out at a range of 4000–750 cm^{-1}, equipped with a continuum microscope and ATR objective. ^{1}HNMR spectra was obtained by a Bruker AVANCE IIIT 600HD spectrometer at 500 MHz using D_2O as solvent.

Mechanical testing

Hydrogels formed in circular molds (D = 8 mm, H = 1/16”) were analyzed using the TA Instruments DMA Q800 Dynamic Mechanical Thermal Analysis (DMTA) in compression mode. The hydrogels were testing at a rate of 0.1 N/min. The strain energy was calculated by measuring the area under the stress-strain curve at 15%. The early or initial strain (< 15%) and late strain (> 25%) moduli, along with the transition strain, were calculated.

Cell culture and encapsulation

Human adipose-derived mesenchymal stem cells (HADMSC, RoosterBio) were cultured as state in the manufacturer’s SOP and used between passage 5–7. Cells were encapsulated in MeGel or mNG with varying amounts of NCC added (0.8% – 2.0%) at a density of 2 million cells/mL with 0.05% Irgacure. All hydrogels were formed at 7% w/v. The gels were molded (D = 4 mm, H = 1/16”), and crosslinked for 5 minutes under UV (365 nm). The cells were cultured either in DMEM/F12 or osteogenic medium (10 mmol/L β- glycerophosphate, 50 mg/mL ascorbic acid, and 10 nmol/L dexamethasone).

Cell viability analysis

A live/dead stain (Invitrogen) and the MTT cell proliferation assay was used to assess cell viability in the hydrogels. For live/dead stain, constructs were incubated in a solution containing 4 mM calcein green AM (Invitrogen) and 2 mM ethidium homodimer-1 (Invitrogen) in 37 °C for 30 minutes. Confocal images were captured using a Zeiss LSM710. Images were quantified using FIJI. In the MTT assay, constructs were incubated in a solution containing 0.5 mg/mL MTT in 37 °C for 4 hours. The insoluble formazan product was solubilized in DMSO for 2 hours and measured using a microplate reader (Bio Tek).

Hydrogel compaction and contraction

Hydrogel discs were imaged periodically for up to 21 days using a Zeiss Discovery V20 SteREO microscope. Images were threshold and processed using FIJI and analyzed using R.

Quantitative PCR

RNA from the hydrogels was extracted using the TRIzol extraction method and reverse transcribed to cDNA using the qScript cDNA SuperMix (Quanta Biosciences). Real-time quantitative PCR was performed using the SYBR Green master mix (QIAGEN). The primers used are listed in Table 2.

Tissue Biochemical analysis

Double stranded DNA (dsDNA), sulfated glycosaminoglycans (sGAGs), and hydroxyproline were measured via PicoGreen kit (Thermo Fisher), dimethylmethylene blue assay (DMMB) [30], and 4-(dimethylamino)benzaldehyde (DMAB)[31] assay, respectively, in native and decellularized tissues. For PicoGreen and DMMB assays, lyophilized samples were digested in papain solution for 16 hours before proceeding. Samples were prepared in 96-well plates and read at 520 nm (excited at 480 nm) for PicoGreen and 656 nm for DMMB. For the DMAB assay, tissues were hydrolyzed in 4.8 N HCl for 3 hours and dried in an oven before proceeding. Samples in the 96-well plate were measured at 550 nm.

3D bioprinting

A Scientist 3D printer (Seraph Robotics) was used for the 3D printing experiments. The bioink used was composed of 10% 0.8 mNG, 5% alginate, and 2 million HADMSC/mL. The composite bioink was loaded into a 10cc syringe (Nordson EFD) with a 20 G needle tip (Nordson EFD). A tubular construct was modeled in AutoCad Fusion 360 and loaded into Slic3r to create print paths. The sizes of the printed products are set as follows: d = 20 mm, h = 15 mm, t = 3 mm. The pressure controlling deposition rate was manually adjusted for each print to ensure consistent deposition rate. Throughout the print, a high-power UV LED system (365 nm) was used to crosslink the printed hydrogel. The printed construct was further crosslinked using 4% calcium chloride for 4 minutes. The constructs were statically cultured for up to 14 days and evaluated using the live-dead assay.

Statistics

All statistics were performed in R using ANOVA and Tukey's HSD post-hoc test. Significance was determined when $P < 0.05$. Error bars represent mean ± standard deviation.

RESULTS

mNG synthesis and characterization

The chemical structures of the samples were characterized by ATR-FTIR spectroscopy and the IR spectra of MeGel, mNCC and mNG are shown in Figure 2. Compared with the spectrum of MeGel, a wider and stronger adsorption was observed at 3300 cm^{-1} in the spectrum of mNG, which mainly belong to the stretching frequency of –OH group in mNCC and C-NH_2 in MeGel. Another obvious difference appeared at 1057 cm^{-1} and 1330 cm^{-1}. The former is assigned to the stretching vibration of CH–O–CH_2 of carboxymethyl group in mNCC, while the latter is corresponded to stretching vibration of –OH. The peak at 1057 cm^{-1} indicating the CH–O–CH_2 stretching vibration of mNCC was present in both the mNCC and mNG samples but not the MeGel.

The ^{1}H NMR spectrum of mNG was recorded in D_2O (Figure 2). Compared with MeGel, there are several new proton signals were observed in the mNG samples at δ 0.9 ppm, 2.73 ppm, and 2.96 ppm that represent protons on the mNCC backbone. The single peak was observed at δ 2.73 ppm which is attributed to the methylene protons of carboxymethyl group in mNG and the peaks at δ 2.96 ppm may be attributed to –CH proton at C4 of mNCC. Besides, the peaks around δ 3.23–3.81 ppm (especially a new peak observed at 3.5) were observed belongs to the –CH ring of mNCC backbone (C 1–5). These results confirmed the conjugation of mNCC and MeGel was successful.

From the results of FTIR and ^{1}HNMR, it can be inferred that that mNCC to MeGel was successfully conjugated to form mNG according to the design.

Mechanical properties

To evaluate the mechanical effects of conjugating mNCC onto the MeGel backbone, the hydrogels were tested under unconfined compression. All hydrogels exhibited nonlinear stress-strain curves, but conjugation of mNCC resulted in a stiffer hydrogel (Figure 3). It

can be seen that an increase in mechanical properties of the mNG with increasing mNCC conjugation, particularly in the strain energy, transition modulus, and the elastic modulus. Incorporating higher concentrations of mNCC resulted in a trend of higher strain energy and toe region (as measured by the strain of the transitional modulus) compared to MeGel, with only the 2.0 mNG showing significant differences (73.8 ± 32.7 kPa vs. 178.0 ± 65.8 kPa and 22.4 ± 5.4% vs. 30.4 ± 1.7%, respectively) (Figure 3A–B). The initial compressive moduli of mNG groups were higher than that of MeGel except for 0.2 mNG (Figure 3C). The transitional and maximum moduli showed similar trends as the strain energy, with 2.0 mNG displaying the largest modulus (0.34 ± 0.09 kPa and 22.1 ± 7.4 kPa, respectively) (Figure 3D–E).

The mass swelling ratios and cell-mediated compaction of the hydrogels were observed (Figure 4). MeGel showed significantly lower swelling ratio at day 7 (10.8 ± 0.9) but the swelling ratio at day 14 was not significantly different from its initial time point. Conversely, the 0.8 mNG (11.1 ± 1.8) had significantly lower swelling ratio while the 1.5 mNG (22.3 ± 2.9) showed higher swelling ratio. The 2.0 mNG did not show any significant changes. The area ratio, a measure for cell-mediated compaction, of 0.8 mNG (0.97 ± 0.02) and 2.0 mNG (0.98 ± 0.06) were similar to that of MeGel (0.87 ± 0.03) by 14 days, but 1.5 mNG swelled the most over time with an area ratio of 1.3 ± 0.02. In all cases, the gels were not significantly different between 7 and 14 days.

Biocompatibility and cell morphology

Cell spreading is critical inside tissue engineered heart valves because spread cells conform to the native valvular interstitial cell morphology and help remodel the matrix. Incorporating nanocellulose enhanced cell spreading in a concentration-dependent manner and showed increased in metabolic activity over time. The high aspect ratio of NCC could be helpful to enhance cell spreading. In live/dead images, cells appeared to be more spread in mNG conditions than in MeGel alone (Figure 5). The percentage of cells spreading increased with increasing concentration of mNG, with the 2.0 mNG showing the most cell spreading. The cells were significantly more metabolically in mNG hydrogel culture between 7 and 14 days compared to the other groups. While the metabolic activity was initially lower than MeGel, the cells within the mNG hydrogels showed the most improvement over time and reached the same level of MeGel alone, supporting high biocompatibility.

ECM deposition

Quantification of sulfated glycosaminoglycans, hydroxyproline, and DNA is shown in Figure 6. MeGel showed little or no GAG deposition. It can be seen that the mNG conditions showed high GAG values, and GAG seem to show a trend of increasing value over time in the mNG conditions. An Alcian blue stain was used to qualify GAG deposition (Figure 7). The normalized ratio of the grey value between the blue and red channels show an increasing blue ratio with increasing concentration of NCC conjugation. The 1.5 mNG and 2.0 mNG, while not significantly different from each other, both show the highest blue/red channel grey ratio value of approximately 1.5.

The amount of hydroxyproline almost unchanged between day 7 and 14 for MeGel. However, there was a decreasing trend within the mNG conditions between the same time points. Moreover, the mNG conditions at day 14 showed lower hydroxyproline content compared to MeGel. These results corroborate with the increase in MMP1 gene expression and the trend of decreasing HYP concentration after 14 days, potentially indicating the start of a remodeling phase.

Phenotyping

The encapsulated MSCs were evaluated for differentiation markers, particularly for myofibroblastic activation and chondrogenic differentiation. The expression of myofibroblastic markers is shown in Figure 8. SMA expression was significantly downregulated within mNG hydrogels (0.44 ± 0.09, 0.40 ± 0.11, and 0.22 ± 0.04 fold change in 0.8, 1.5, and 2.0 mNG, respectively) compared to MeGel, and the expression level did not change over time. Conversely, vimentin was upregulated in mNG hydrogels after 14 days in culture (1.6 ± 0.5, 2.8 ± 0.4, and 4.3 ± 0.9 fold change in 0.8, 1.5, and 2.0 mNG, respectively). Generally, encapsulated cells are activated and display a myofibroblastic phenotype (SMA+) within MeGel.[12],[32]

The expression of MMP1 was low during early time points but became upregulated after 14 days compared within the same hydrogel conditions but were not significantly different from MeGel. However, while MMP1 was upregulated over time, MMP2 showed the opposite effect, showing down regulation of approximately 0.50-fold change in all mNG hydrogels after 14 days compared to the early time points. The results demonstrated that incorporation of mNCC induced and maintained HADMSC differentiation to a quiescent fibroblast phenotype in a concentration-dependent manner.

The expression of chondrogenic markers is shown in Figure 8. In mNG hydrogels, SMA expression was decreased while vimentin expression increased over time. MMP1 increased while MMP2 decreased over time. ACAN was significantly increased compared to MeGel in all time points and showed an increase in expression between days 3 and 14 in the mNG hydrogels (15.4 ± 2.2, 15.4 ± 2.9, and 19.0 ± 2.9fold change in 0.8, 1.5, and 2.0 mNG, respectively). Sox9 was upregulated initially for 0.8mNG and 1.5 mNG but decreased in expression after 14 days. However, the 2.0 mNG condition showed an increase in Sox9 expression. These results support the HADMSC adopting a chondrogenic phenotype.

Phenotypic changes in osteogenic media

Calcification is a hallmark of advanced valvular disease where valve interstitial cells become osteogenic-like and deposit bone-like matrix. To evaluate the osteogenic potential of this material, the HADMSC encapsulated within the hydrogels were challenged with OGM and evaluated for osteogenic markers. The osteogenic potential of mNG samples were compared to MeGel, which has been shown to induce osteogenic differentiation.[33]

The encapsulated HADMSC initially showed a myofibroblastic or activated phenotype in the 1.5 and 2.0 mNG hydrogels, as evident by the upregulation in SMA in day 7 (3.5 ± 1.1 and 3.7 ± 1.7 fold change, respectively) (Figure 9). SMA was decreased in 0.8 mNG but increased in 1.5mNG and 2.0 mNG. Vimentin showed decrease in 1.5mNG and 2.0

mNG over time. By day 14, the SMA expression were similar to the MeGel condition. Interestingly, only the 0.8 mNG showed a downregulation of SMA for both time points with a 0.40 ± 0.06fold change. Vimentin expression was similar between conditions except for the downregulation in the 1.5 and 2.0 mNG conditions at the later time point (0.52 ± 0.18 and 0.34 ± 0.05fold change, respectively).

Gene identifiers for osteogenic differentiation, including Runx2 and osteocalcin, were evaluated. Runx2 is a transcription factor closely related to early stage osteogenic differentiation.[34],[35] Osteocalcin is a protein needed for bone mineralization and is promoted by the presence of Runx2.[36] After 14 days in culture, Runx2 and OCN were downregulated in mNG hydrogels compared to the MeGel by approximately 0.5-fold change in all conditions. The trends hold true when comparing between GM and OGM media conditions in the same hydrogels at day 14 (Figure 10). Runx2 expression increased within the mNG hydrogels under OGM conditions, but the overall expression was significantly lower compared to MeGel. Similarly, the expression of OCN was lower within the mNG hydrogels in both GM and OGM conditions. No significant differences were observed in the OPN expression levels between the GM and OGM groups. (* $P < 0.05$ compared to MeGel in the same media condition, # $P < 0.05$ compared to GM within the same hydrogel group, N = 3–4). To further evaluate osteogenic differentiation, the hydrogels were stained with alizarin red, which stains calcium-rich regions red (Figure 11). The D14 hydrogels did not appear different between the GM and OGM conditions, but MeGel appeared more stained than the mNG hydrogels. While there was no observable nodule formation in any hydrogels, the deeply stained region of MeGel demonstrate a more susceptible environment for osteogenesis to occur, and the results support that encapsulated HADMSC within mNG hydrogels has less osteogenic potential than in MeGel.

3D bioprinting with mNG-laden bioink

As a proof of concept for tissue fabrication with mNG, the mNG was mixed with alginate to form a bioink and used to 3D bioprint a construct (Figure 12). The 0.8 mNG yielded the highest fidelity based on the grid pattern, so the remainder of the prints used the 0.8 mNG as the base polymer. From the prints, we showed a tall, multi-layered, self-standing tubular construct was achievable. After culturing for 7 days, the resulting tube swelled slightly without any signs of delamination from the printing process, and the live/dead images and quantification show viable cells.

DISCUSSION

Calcific heart valve disease is an increasing global problem affecting patients of all ages[37], and as a result, heart valve replacement surgery is estimated to triple by 2050.[38] Tissue engineering heart valve is a promising choice for replacing diseased or injured heart valves because of its ability to integrate and grow with the patient. However, common materials used for fabricating tissues, such as methacrylated gelatin, can become calcify or result in a fibrotic tissue, leading to leaflet retraction or stenosis.[10],[14],[39] Nanocellulose have been used in engineering tissues, commonly for cartilage and ligament engineering, because of the material’s ability to swell, differentiate cells towards a chondrogenic lineage, and

increase mechanical properties.[20],[21],[22],[24] Understanding the unique properties each material possess for heart valve tissue engineering, we sought to combine the two together to synthesize a new composite biomaterial. Here, we present for the first time the conjugation of TEMPO-modified nanocrystalline cellulose onto the backbone of methacrylated gelatin. The composite biomaterial mNG enhanced material mechanics and cell spreading. Stem cells encapsulated within the mNG hydrogel adopted a quiescent fibroblastic phenotype and displayed phenotypic properties found within the spongiosa of the heart valve. Lastly, the mNG hydrogel protected against osteogenic differentiation of the encapsulated stem cells. Based on these properties, the composite hydrogel is promising for tissue engineering heart valves.

mNG characterization

Incorporation of nanocellulose has been used in tissue engineering applications, particularly to enhance mechanical strength. Incorporating NCC via chemical or physical entrapment have been shown to increase both the compressive modulus and swelling in numerous hydrogel systems, including polyvinyl alcohols, polyacrylamide/polyacrylates, and natural polymers.[27] NCC can form both intra- and inter-molecular hydrogen bonding, thus enhancing the composite materials.[20],[40] In fiber-reinforced composite materials, there is an optimum fiber fraction volume for maximizing mechanical properties, and deviation from the optimum can decrease overall strength.[41] Unlike other groups that have mixed nanocellulose with another material to make a fiber-reinforced composite material[42], our composite biomaterial contains only one bulk material with different degree of nanocellulose conjugation rather than mixing multiple materials. Conjugating more mNCC onto the backbone of MeGel would result in more hydrogen bonding, thus enhancing material strength by formation of an interpenetrating network. We would not expect the material to weaken at lower or higher degree of NCC conjugation because the fractions are part of the MeGel backbone and not physically entrapped. From our data, we saw an increase in mechanical properties of the mNG with increasing mNCC conjugation, particularly in the strain energy, initial strain modulus, transition strain, and the late strain (elastic) modulus. The enhanced mechanical compressive strength would aid in engineering the fibrosa layer, which resists the high aortic pressure during diastole. Additionally, the swelling could be useful in engineering the GAG-rich spongiosa layer or reducing cell-mediated compaction of hydrogels that have plagued other engineered valves.[43],[44] The enhanced mechanical strength via addition of more mNCC needs to be carefully balanced for heart valve tissue engineering. Compared to PEGDA that our group have previously used to form 3D printed aortic heart valves[45], the strong non-linear stiffening observed with the mNG provides low stiffness at physiological strains for heart valve cells but protective stiffening at higher pressures. The resisting deformation under higher pressures may facilitate greater elastic recoil. While engineering a high-strength tissue is useful to prevent disintegration in vivo, too high of stiffness could provide environments for cells to become disease-like and become osteogenic and calcify.[46],[47]

Effect of mNG on cell biocompatibility and phenotype

Cell alignment can be an important attribute as well for engineering valves, specifically for the fibrosa and ventricularis layers, and nanocellulose can be used for achieving cellular

alignment. Fabrication technique is crucial in producing aligned microarchitecture on which cells can align. The length scale of the nanocellulose is smaller than the cells, but because the nanocellulose is conjugated on the backbone of a larger polymer, MeGel, alignment of mNG is possible.[48],[49],[50],[51] Mechanical stimulation can help induce alignment, particularly in cyclic compression or tension to mimic the diastolic or systolic phases, respectively.[52]

Nanocellulose exhibits low affinity for cell attachment, but coupled with a base polymer, the composite can modulate cell behavior. In this case, methacrylated gelatin was chosen to provide cell adhesion points for the cells to grow and mechanical tunability. Generally, encapsulated cells are activated and display a myofibroblastic phenotype (SMA+) within MeGel.[12],[32] Interestingly, the conjugation of mNCC lowered the expression of SMA while increasing vimentin expression, thus supporting a pro-quiescent fibroblastic phenotype of the HADMSC. Others have shown similar properties of nanocellulose hydrogels decreasing in myofibroblastic activation by decrease in SMA expression, particularly for in vivo wound healing, potentially by modulating factors (e.g. TGF-β).[53],[54],[55]

The initial promotion of a chondrogenic phenotype of the HADMSC within mNG hydrogels may be suited for engineering the GAG-rich layer. Additionally, the swelling could be useful in reducing cell-mediated compaction of hydrogels that have plagued other engineered valves.[43],[44] However, mNG should eventually promote a quiescent, non-chondrogenic, and non-myofibroblastic population of cells to prevent over production and accumulation of GAG, which could lead to a myxomatous-like scaffold[56], and overly-contractile matrix, which could lead to a fibrotic and stiff scaffold.[57] Based on the cell phenotype results, the mNG material induced early remodeling and late maturation.

Additionally, nanocellulose has been used in the context for cartilage engineering, particularly by forming hydrogels either alone or in combination with other materials through physical entrapment.[20] These nanocellulose-laden hydrogels can induce neocartilage formation[58], maintain chondrogenic phenotype, and promote chondrogenic redifferentiation.[59] Cells within these scaffolds deposited more GAG and collagen and expressed higher levels of chondrogenic genes, including ACAN and Sox9. In our hydrogel system, instead of physical entrapment, we conjugated nanocellulose to the MeGel backbone to formulate mNG hydrogels. The HADMSC encapsulated within mNG in our study behaved similarly to other cells seeded in nanocellulose-laden hydrogels, suggesting that mNG may initially promote a chondrogenic phenotype, particularly based on the upregulation of ACAN and Sox9 during early time points. However, the downregulation of myofibroblastic genes (SMA, MMP2) and the upregulation Vim may indicate more of a fibroblastic phenotype of the HADMSC.

Lastly, the nanocellulose-laden hydrogels showed downregulation of some osteogenic markers when compared to MeGel, which is a material that can promote osteogenic differentiation. However, in the context of heart valve engineering, osteogenic differentiation and calcium deposition should be minimized. Nanocellulose has been used by several groups to make nanocellulose hydrogel composites with collagen, hydroxyapatite, and/or calcium phosphate to induce osteogenic differentiation or maintain osteogenic phenotype.

[60],[61] Additionally, another group has reported MSC in bacterial nanocellulose can stimulate MSC towards osteogenic lineage without addition of inorganic materials into the hydrogel, showing positive alkaline phosphatase staining.[62] Based on the results, incorporating mNCC is inhibitory of osteogenic differentiation of HADMSC, particularly with Runx2 and osteocalcin. Although the mechanism of inhibition is not currently known, it could be attributed to incorporating nanocellulose, which can induce chondrogenic differentiation without the aid of growth factors via surface roughness or the availability of glucose monomers via degradation. [63].

The results show promising phenotypic changes of the encapsulated HADMSC within the mNCC towards the cell types needed for TEHV, but additional studies are needed to fully develop the cell type and tissue architecture of the heart valve. The study was conducted in static culture, and dynamically culturing the hydrogels within a bioreactor system would provide further mechanical cues to aid in cell differentiation, protein secretion, and matrix development. The fold changes observed, while statistically significant, were generally under two-fold difference, but additional bioreactor studies mimicking in vivo conditions may increase the observed differences.

3D bioprinting with mNG-laden bioink

The main goal is to use the mNG biomaterial to fabricate TEHV. We have shown the low-viscosity formulation of mNG can be casted into custom molds and crosslinked via UV. Additionally, as a proof of concept, we incorporated mNG into a bioink for 3D bioprinting applications. To increase viscosity, alginate was added with the mNG to ensure it can be extruded.

Several researchers have already reported printing with a mixture of nanocellulose (i.e. physical entrapment) and alginate with varying degree of success.[59],[64],[65] In many of these studies, cells adopted a round morphology shape, potentially due to either the lack of adhesion molecules or the high matrix density. These properties that result in round cell morphology are ideal for cartilage engineering because chondrocytes normally have a rounded morphology, but in heart valve engineering, interstitial cells normally have a spindle-like morphology. Xu et al. printed using a blend of NFC and low concentration of MeGel without chemical conjugation and showed feasibility of printing a small grid, but the 3T3 fibroblasts remained rounded after 72 hours of growth.[42] Conversely, Müller et al. showed cell spreading of primary articular chondrocytes in alginate sulfate-bacterial nanocellulose after a minimum of 14 days and depended on the tip size.[64] Here, we showed the feasibility of bioprinting a tall, self-standing tubular structure with viable cells over a period of 7 days. Similar to past studies, the cell morphology was also relatively round. However, the culture period was relatively short (7 days vs 14 days), but given a longer culture period, we would expect the cells to start remodeling the matrix and begin spreading, particularly because of the presence of adhesion motifs found on the MeGel backbone. The mNG hybrid hydrogel, combined with alginate or other viscosity modifier, could provide a foundational bioink for TEHV applications.

CONCLUSION

A new composite hydrogel was fabricated by conjugating mNCC to the MeGel backbone to form mNG for tissue engineering applications. Encapsulated HADMSC in the mNG hydrogels were bioactive and displayed more cell spreading. They adopted a quiescent fibroblastic phenotype and displayed phenotypic properties found within the spongiosa of the heart valve. The hydrogels displayed nonlinear biomechanics and could be useful for engineering the fibrosa or spongiosa layers due to the enhanced mechanical properties and environment for GAG-deposition and lower propensity for calcification. Moreover, the 3D bioprinting construct of the mNG biomaterial with HADMSC showed viable cells after culturing for 7 days. This study showed the feasibility of using mNG as a biomaterial to potentially be used to engineer multiple layers the heart valve.a

ACKNOWLEDGEMENTS

This work was funded by the National Institutes of Health (NIH R21AR070408, NIH HL128745), NSF Graduate Research Fellowship (DGE-1650441), and HHMI Fellowship (56006761) and by the Program of Guangdong Academy of Sciences (2017GDASCX-0503, 2018GDASCX-0105). Imaging data was acquired through the Cornell Institute of Biotechnology's Imaging Facility supported with NIH 1S10OD010605 funding.

REFERENCES

[1]. Nishimura RA, Grantham JA, Connolly HM, Schaff HV, Higano ST, Holmes DR. Low-output, low-gradient aortic stenosis in patients with depressed left ventricular systolic function - The clinical utility of the dobutamine challenge in the catheterization laboratory. Circulation. 2002;106:809–13. [PubMed: 12176952]

[2]. Benjamin EJ, Muntner P, Alonso A, Bittencourt MS, Callaway CW, Carson AP, et al. Heart Disease and Stroke Statistics-2019 Update A Report From the American Heart Association. Circulation. 2019;139:E56–E528. [PubMed: 30700139]

[3]. Carapetis JR, McDonald M, Wilson NJ. Acute rheumatic fever. Lancet. 2005;366:155–68. [PubMed: 16005340]

[4]. Lerman DA, Prasad S, Alotti N. Calcific Aortic Valve Disease: Molecular Mechanisms and Therapeutic Approaches. European cardiology. 2015;10:108–12. [PubMed: 27274771]

[5]. Freeman RV, Otto CM. Spectrum of calcific aortic valve disease - Pathogenesis, disease progression, and treatment strategies. Circulation. 2005;111:3316–26. [PubMed: 15967862]

[6]. Reineke D, Gisler F, Englberger L, Carrel T. Mechanical versus biological aortic valve replacement strategies. Expert review of cardiovascular therapy. 2016;14:423–30. [PubMed: 26678683]

[7]. Chiang YP, Chikwe J, Moskowitz AJ, Itagaki S, Adams DH, Egorova NN. Survival and Long-term Outcomes Following Bioprosthetic vs Mechanical Aortic Valve Replacement in Patients Aged 50 to 69 Years. Jama-Journal of the American Medical Association. 2014;312:1323–9.

[8]. Alsoufi B Aortic valve replacement in children: Options and outcomes. Journal of the Saudi Heart Association. 2014;26:33–41. [PubMed: 24578598]

[9]. Sharabiani MTA, Dorobantu DM, Mahani AS, Turner M, Tometzki AJP, Angelini GD, et al. Aortic Valve Replacement and the Ross Operation in Children and Young Adults. Journal of the American College of Cardiology. 2016;67:2858–70. [PubMed: 27311525]

[10]. Nichol JW, Koshy ST, Bae H, Hwang CM, Yamanlar S, Khademhosseini A. Cell-laden microengineered gelatin methacrylate hydrogels. Biomaterials. 2010;31:5536–44. [PubMed: 20417964]

[11]. Duan B, Kapetanovic E, Hockaday LA, Butcher JT. Three-dimensional printed trileaflet valve conduits using biological hydrogels and human valve interstitial cells. Acta Biomaterialia. 2014;10:1836–46. [PubMed: 24334142]

[12]. Duan B, Hockaday LA, Kapetanovic E, Kang KH, Butcher JT. Stiffness and adhesivity control aortic valve interstitial cell behavior within hyaluronic acid based hydrogels. Acta Biomaterialia. 2013;9:7640–50. [PubMed: 23648571]

[13]. Billiar KL, Sacks MS. Biaxial mechanical properties of the natural and glutaraldehyde treated aortic valve cusp - Part I: Experimental results. Journal of Biomechanical Engineering-Transactions of the Asme. 2000;122:23–30.

[14]. Celikkin N, Mastrogiacomo S, Jaroszewicz J, Walboomers XF, Swieszkowski W. Gelatin methacrylate scaffold for bone tissue engineering: The influence of polymer concentration. Journal of Biomedical Materials Research Part A. 2018;106:201–9. [PubMed: 28884519]

[15]. Joy J, Pereira J, Aid-Launais R, Pavon-Djavid G, Ray AR, Letourneur D, et al. Gelatin - Oxidized carboxymethyl cellulose blend based tubular electrospun scaffold for vascular tissue engineering. International Journal of Biological Macromolecules. 2018;107:1922–35. [PubMed: 29032216]

[16]. Jiang Y, Xv X, Liu D, Yang Z, Zhang Q, Shi H, et al. Preparation of Cellulose Nanofiber-reinforced Gelatin Hydrogel and Optimization for 3D Printing Applications. Bioresources. 2018;13:5909–24.

[17]. Hivechi A, Bahrami SH, Siegel RA. Investigation of morphological, mechanical and biological properties of cellulose nanocrystal reinforced electrospun gelatin nanofibers. International Journal of Biological Macromolecules. 2019;124:411–7. [PubMed: 30476513]

[18]. Weber C, Reinhardt S, Eghbalzadeh K, Wacker M, Guschlbauer M, Maul A, et al. Patency and in vivo compatibility of bacterial nanocellulose grafts as small-diameter vascular substitute. Journal of Vascular Surgery. 2018;68:177S–87S. [PubMed: 29248244]

[19]. Cherian BM, Leao AL, de Souza SF, Manzine Costa LM, de Olyveira GM, Kottaisamy M, et al. Cellulose nanocomposites with nanofibres isolated from pineapple leaf fibers for medical applications. Carbohydrate Polymers. 2011;86:1790–8.

[20]. Lin N, Dufresne A. Nanocellulose in biomedicine: Current status and future prospect. European Polymer Journal. 2014;59:302–25.

[21]. Muller FA, Muller L, Hofmann I, Greil P, Wenzel MM, Staudenmaier R. Cellulose-based scaffold materials for cartilage tissue engineering. Biomaterials. 2006;27:3955–63. [PubMed: 16530823]

[22]. Bodin A, Concaro S, Brittberg M, Gatenholm P. Bacterial cellulose as a potential meniscus implant. Journal of Tissue Engineering and Regenerative Medicine. 2007;1:406–8. [PubMed: 18038435]

[23]. Bacakova L, Pajorova J, Bacakova M, Skogberg A, Kallio P, Kolarova K, et al. Versatile Application of Nanocellulose: From Industry to Skin Tissue Engineering and Wound Healing. Nanomaterials. 2019;9:164–202.

[24]. Hickey RJ, Pelling AE. Cellulose Biomaterials for Tissue Engineering. Frontiers in Bioengineering and Biotechnology. 2019;7:45–59. [PubMed: 30968018]

[25]. Millon LE, Wan WK. The polyvinyl alcohol-bacterial cellulose system as a new nanocomposite for biomedical applications. Journal of Biomedical Materials Research Part B-Applied Biomaterials. 2006;79B:245–53.

[26]. Wang K, Nune KC, Misra RDK. The functional response of alginate-gelatin-nanocrystalline cellulose injectable hydrogels toward delivery of cells and bioactive molecules. Acta Biomaterialia. 2016;36:143–51. [PubMed: 26971665]

[27]. De France KJ, Hoare T, Cranston ED. Review of Hydrogels and Aerogels Containing Nanocellulose. Chemistry of Materials. 2017;29:4609–31.

[28]. Lin N, Bruzzese C, Dufresne A. TEMPO-Oxidized Nanocellulose Participating as Crosslinking Aid for Alginate-Based Sponges. Acs Applied Materials & Interfaces. 2012;4:4948–59. [PubMed: 22950801]

[29]. Sacui IA, Nieuwendaal RC, Burnett DJ, Stranick SJ, Jorfi M, Weder C, et al. Comparison of the Properties of Cellulose Nanocrystals and Cellulose Nanofibrils Isolated from Bacteria, Tunicate, and Wood Processed Using Acid, Enzymatic, Mechanical, and Oxidative Methods. Acs Applied Materials & Interfaces. 2014;6:6127–38. [PubMed: 24746103]

[30]. Farndale RW, Sayers CA, Barrett AJ. A DIRECT SPECTROPHOTOMETRIC MICRO-ASSAY FOR SULFATED GLYCOSAMINOGLYCANS IN CARTILAGE CULTURES. Connective Tissue Research. 1982;9:247–8. [PubMed: 6215207]

[31]. Reddy GK, Enwemeka CS. A simplified method for the analysis of hydroxyproline in biological tissues. Clinical Biochemistry. 1996;29:225–9. [PubMed: 8740508]

[32]. Hjortnaes J, Goettsch C, Hutcheson JD, Camci-Unal G, Lax L, Scherer K, et al. Simulation of early calcific aortic valve disease in a 3D platform: A role for myofibroblast differentiation. Journal of Molecular and Cellular Cardiology. 2016;94:13–20. [PubMed: 26996755]

[33]. Yue K, Trujillo-de Santiago G, Moises Alvarez M, Tamayol A, Annabi N, Khademhosseini A. Synthesis, properties, and biomedical applications of gelatin methacryloyl (GelMA) hydrogels. Biomaterials. 2015;73:254–71. [PubMed: 26414409]

[34]. Graneli C, Thorfve A, Ruetschi U, Brisby H, Thomsen P, Lindahl A, et al. Novel markers of osteogenic and adipogenic differentiation of human bone marrow stromal cells identified using a quantitative proteomics approach. Stem Cell Research. 2014;12:153–65. [PubMed: 24239963]

[35]. Komori T Regulation of Osteoblast Differentiation by Runx2. In: Choi Y, editor. Osteoimmunology: Interactions of the Immune and Skeletal Systems Ii2010. p. 43–9.

[36]. Birmingham E, Niebur GL, McHugh PE, Shaw G, Barry FP, McNamara LM. OSTEOGENIC DIFFERENTIATION OF MESENCHYMAL STEM CELLS IS REGULATED BY OSTEOCYTE AND OSTEOBLAST CELLS IN A SIMPLIFIED BONE NICHE. European Cells & Materials. 2012;23:13–27. [PubMed: 22241610]

[37]. Coffey S, Cairns BJ, Iung B. The modern epidemiology of heart valve disease. Heart. 2016;102:75–85. [PubMed: 26541169]

[38]. Yacoub N, Takkenberg J. Will heart valve tissue engineering change the world? Nature Clinical Practice Cardiovascular Medicine. 2005;2:60–1.

[39]. Ghanbari H, Viatge H, Kidane AG, Burriesci G, Tavakoli M, Seifalian AM. Polymeric heart valves: new materials, emerging hopes. Trends in Biotechnology. 2009;27:359–67. [PubMed: 19406497]

[40]. Nishiyama Y Molecular interactions in nanocellulose assembly. Philosophical Transactions of the Royal Society a-Mathematical Physical and Engineering Sciences. 2018;376.

[41]. McCarthy C, Vaughan T. Micromechanical failure analysis of advanced composite materials. Numerical Modelling of Failure in Advanced Composite Materials2015. p. 379–409.

[42]. Xu W, Molino BZ, Cheng F, Molino PJ, Yue Z, Su D, et al. On Low-Concentration Inks Formulated by Nanocellulose Assisted with Gelatin Methacrylate (GelMA) for 3D Printing toward Wound Healing Application. Acs Applied Materials & Interfaces. 2019;11:8838–48. [PubMed: 30741518]

[43]. Flanagan TC, Sachweh JS, Frese J, Schnoering H, Gronloh N, Koch S, et al. In Vivo Remodeling and Structural Characterization of Fibrin-Based Tissue-Engineered Heart Valves in the Adult Sheep Model. Tissue Engineering Part A. 2009;15:2965–76. [PubMed: 19320544]

[44]. Mol A, Driessen NJB, Rutten MCM, Hoerstrup SP, Bouten CVC, Baaijens FPT. Tissue engineering of human heart valve leaflets: A novel bioreactor for a strain-based conditioning approach. Annals of Biomedical Engineering. 2005;33:1778–88. [PubMed: 16389526]

[45]. Hockaday LA, Kang KH, Colangelo NW, Cheung DYC, Duan B, Malone E, et al. Rapid 3D printing of anatomically accurate and mechanically heterogeneous aortic valve hydrogel scaffolds. Biofabrication. 2012;4:1–10.

[46]. Kim DS, Jung S-M, Yoon GH, Lee HC, Shin HS. Development of a complex bone tissue culture system based on cellulose nanowhisker mechanical strain. Colloids and Surfaces B-Biointerfaces. 2014;123:838–44. [PubMed: 25454753]

[47]. Pedrosa CR, Arl D, Grysan P, Khan I, Durrieu S, Krishnamoorthy S, et al. Controlled Nanoscale Topographies for Osteogenic Differentiation of Mesenchymal Stem Cells. Acs Applied Materials & Interfaces. 2019;11:8858–66. [PubMed: 30785254]

[48]. He X, Xiao Q, Lu C, Wang Y, Zhang X, Zhao J, et al. Uniaxially Aligned Electrospun All-Cellulose Nanocomposite Nanofibers Reinforced with Cellulose Nanocrystals: Scaffold for Tissue Engineering. Biomacromolecules. 2014;15:618–27. [PubMed: 24405043]

[49]. Skogberg A, Maki A-J, Mettanen M, Lahtinen P, Kallio P. Cellulose Nanofiber Alignment Using Evaporation-Induced Droplet-Casting, and Cell Alignment on Aligned Nanocellulose Surfaces. Biomacromolecules. 2017;18:3936–53. [PubMed: 28960956]

[50]. Qin H, Zhang T, Li N, Cong H-P, Yu S-H. Anisotropic and self-healing hydrogels with multi-responsive actuating capability. Nature Communications. 2019;10:2202–12.

[51]. Capulli AK, Emmert MY, Pasqualini FS, Kehl D, Caliskan E, Lind JU, et al. JetValve: Rapid manufacturing of biohybrid scaffolds for biomimetic heart valve replacement. Biomaterials. 2017;133:229–41. [PubMed: 28445803]

[52]. Gauvin R, Parenteau-Bareil R, Larouche D, Marcoux H, Bisson F, Bonnet A, et al. Dynamic mechanical stimulations induce anisotropy and improve the tensile properties of engineered tissues produced without exogenous scaffolding. Acta Biomaterialia. 2011;7:3294–301. [PubMed: 21669302]

[53]. Loh EYX, Mohamad N, Fauzi MB, Min Hwei N, Shiow Fern N, Amin MCIM. Development of a bacterial cellulose-based hydrogel cell carrier containing keratinocytes and fibroblasts for full-thickness wound healing. Scientific Reports. 2018;8:2875–86. [PubMed: 29440678]

[54]. Sultana T, Hai HV, Abueva C, Kang HJ, Lee S-Y, Lee B-T. TEMPO oxidized nano-cellulose containing thermo-responsive injectable hydrogel for post-surgical peritoneal tissue adhesion prevention. Materials Science & Engineering C-Materials for Biological Applications. 2019;102:12–21.

[55]. Moniri M, Moghaddam AB, Azizi S, Rahim RA, Zuhainis SW, Navaderi M, et al. In vitro molecular study of wound healing using biosynthesized bacteria nanocellulose/silver nanocomposite assisted by bioinformatics databases. International Journal of Nanomedicine. 2018;13:5097–112. [PubMed: 30254435]

[56]. Levine RA, Hagege AA, Judge DP, Padala M, Dal-Bianco JP, Aikawa E, et al. Mitral valve disease morphology and mechanisms. Nature Reviews Cardiology. 2015;12:689–710. [PubMed: 26483167]

[57]. Liu AC, Joag VR, Gotlieb AI. The emerging role of valve interstitial cell phenotypes in regulating heart valve pathobiology. American Journal of Pathology. 2007;171:1407–18. [PubMed: 17823281]

[58]. Avila HM, Feldmann E-M, Pleumeekers MM, Nimeskern L, Kuo W, de Jong WC, et al. Novel bilayer bacterial nanocellulose scaffold supports neocartilage formation in vitro and in vivo. Biomaterials. 2015;44:122–33. [PubMed: 25617132]

[59]. Martínez ávila H, Schwarz S, Rotter N, Gatenholm P. 3D bioprinting of human chondrocyte-laden nanocellulose hydrogels for patient-specific auricular cartilage regeneration. Bioprinting. 2016;s 1–2:22–35.

[60]. Saska S, Teixeira LN, Spinola de Castro Raucci LM, Scarel-Caminaga RM, Franchi LP, dos Santos RA, et al. Nanocellulose-collagen-apatite composite associated with osteogenic growth peptide for bone regeneration. International Journal of Biological Macromolecules. 2017;103:467–76. [PubMed: 28527999]

[61]. Sundberg J, Gotherstrom C, Gatenholm P. Biosynthesis and in vitro evaluation of macroporous mineralized bacterial nanocellulose scaffolds for bone tissue engineering. Bio-Medical Materials and Engineering. 2015;25:39–52. [PubMed: 25585979]

[62]. Vielreicher M, Kralisch D, Voelkl S, Sternal F, Arkudas A, Friedrich O. Bacterial nanocellulose stimulates mesenchymal stem cell expansion and formation of stable collagen-I networks as a novel biomaterial in tissue engineering. Scientific Reports. 2018;8:9401–14. [PubMed: 29925980]

[63]. Singh N, Rahatekar SS, Koziol KKK, Ng THS, Patil AJ, Mann S, et al. Directing Chondrogenesis of Stem Cells with Specific Blends of Cellulose and Silk. Biomacromolecules. 2013;14:1287–98. [PubMed: 23534615]

[64]. Mueller M, Ozturk E, Arlov O, Gatenholm P, Zenobi-Wong M. Alginate Sulfate-Nanocellulose Bioinks for Cartilage Bioprinting Applications. Annals of Biomedical Engineering. 2017;45:210–23. [PubMed: 27503606]

[65]. Apelgren P, Karabulut E, Amoroso M, Mantas A, Avila HM, Kolby L, et al. In Vivo Human Cartilage Formation in Three-Dimensional Bioprinted Constructs with a Novel Bacterial Nanocellulose Bioink. Acs Biomaterials Science & Engineering. 2019;5:2482–90. [PubMed: 33405755]

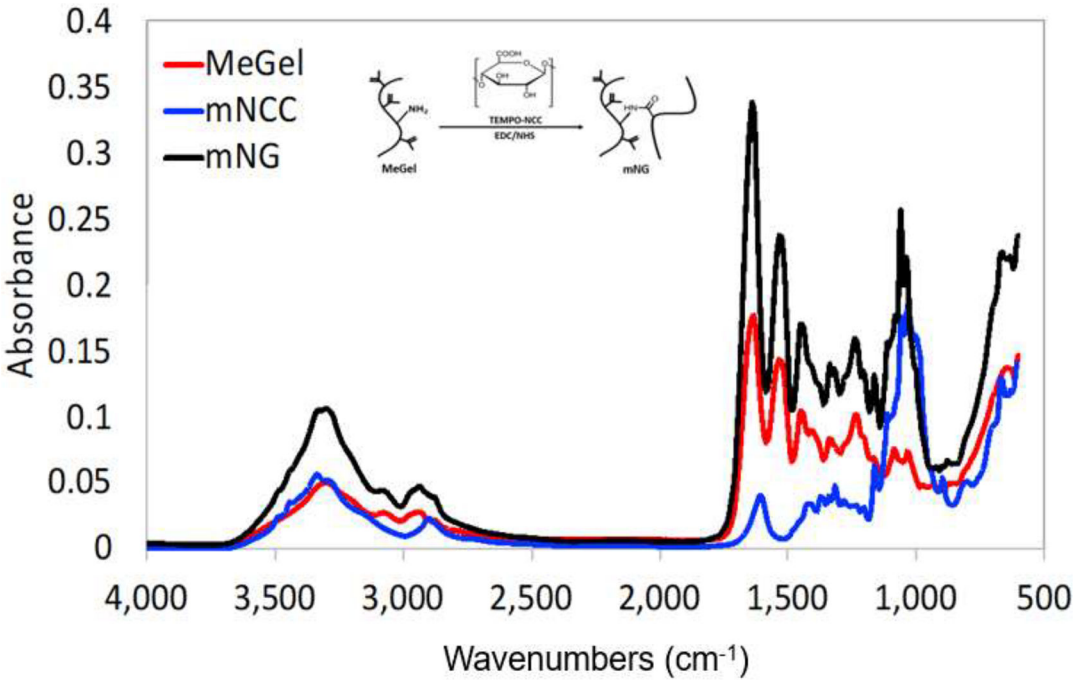

Figure 1.
FTIR spectrum of MeGel (red), mNCC (blue), and mNG (blue).

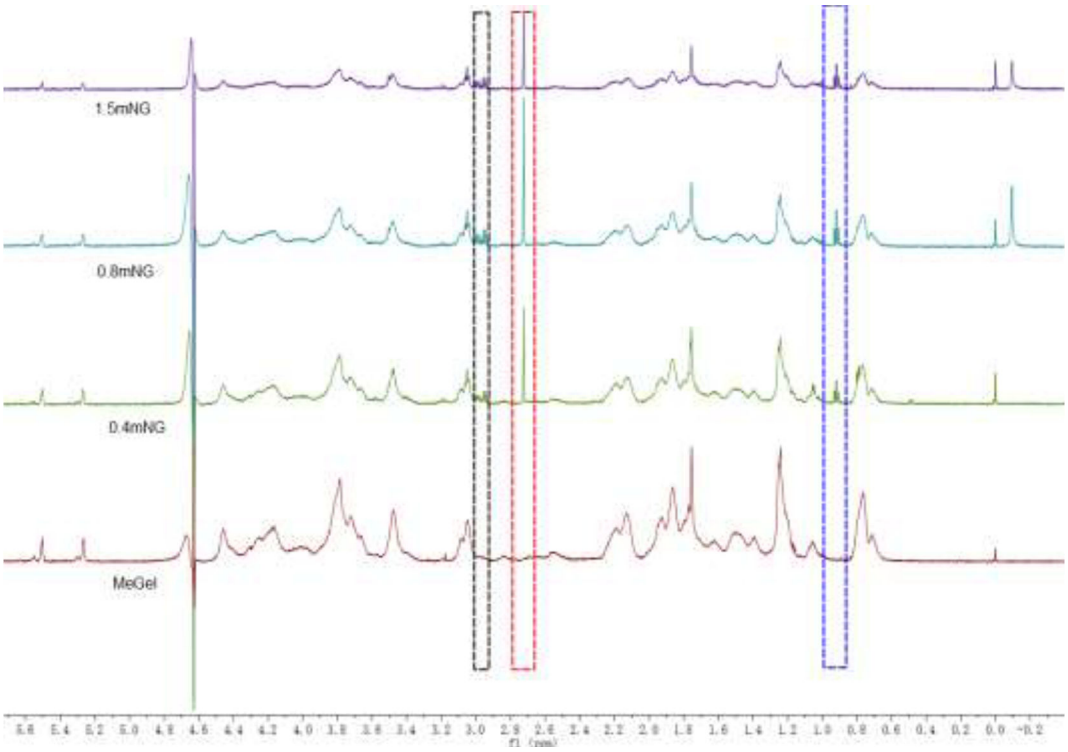

Figure 2.
^{1}H NMR spectra of MeGel and mNG.

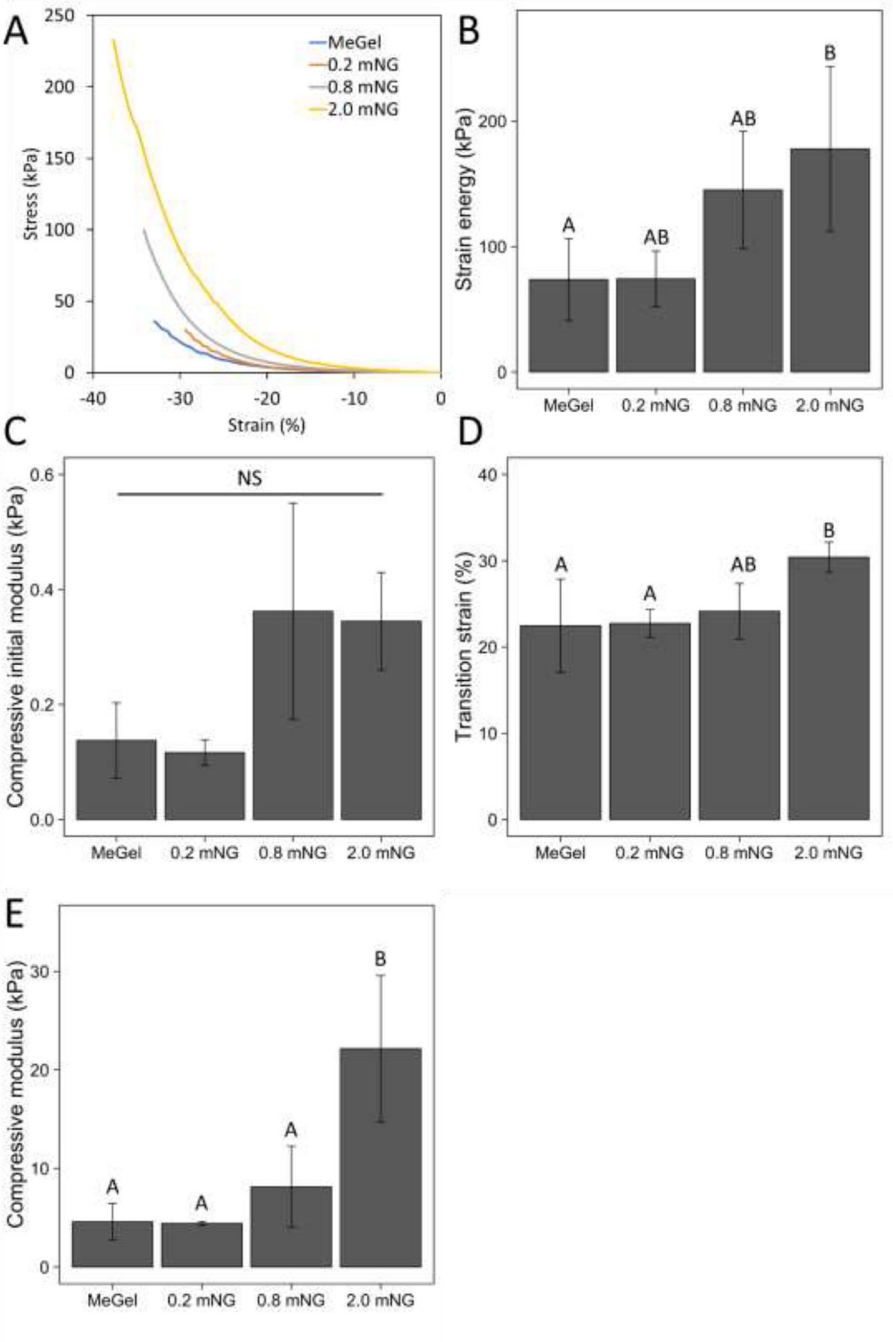

Figure 3.

Unconfined compression of MeGel and mNG. (A) A representative stress-strain curve of MeGel and mNG; (B) Strain energy; (C)Compressive initial modulus (< 15 %) (D) Transition strain (> 25%) (E) Compressive modulus (> 25%).

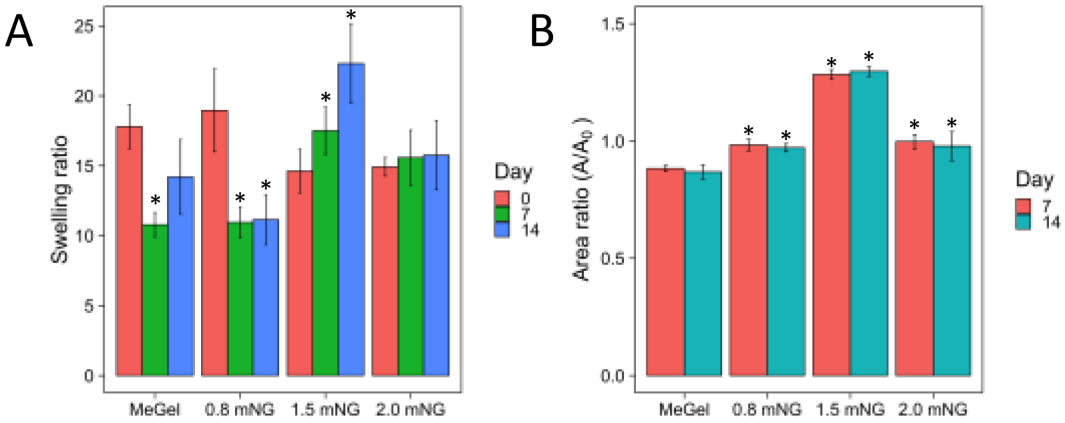

Figure 4.
The mass swelling ratio and compaction behavior of MeGel and mNG hydrogels.

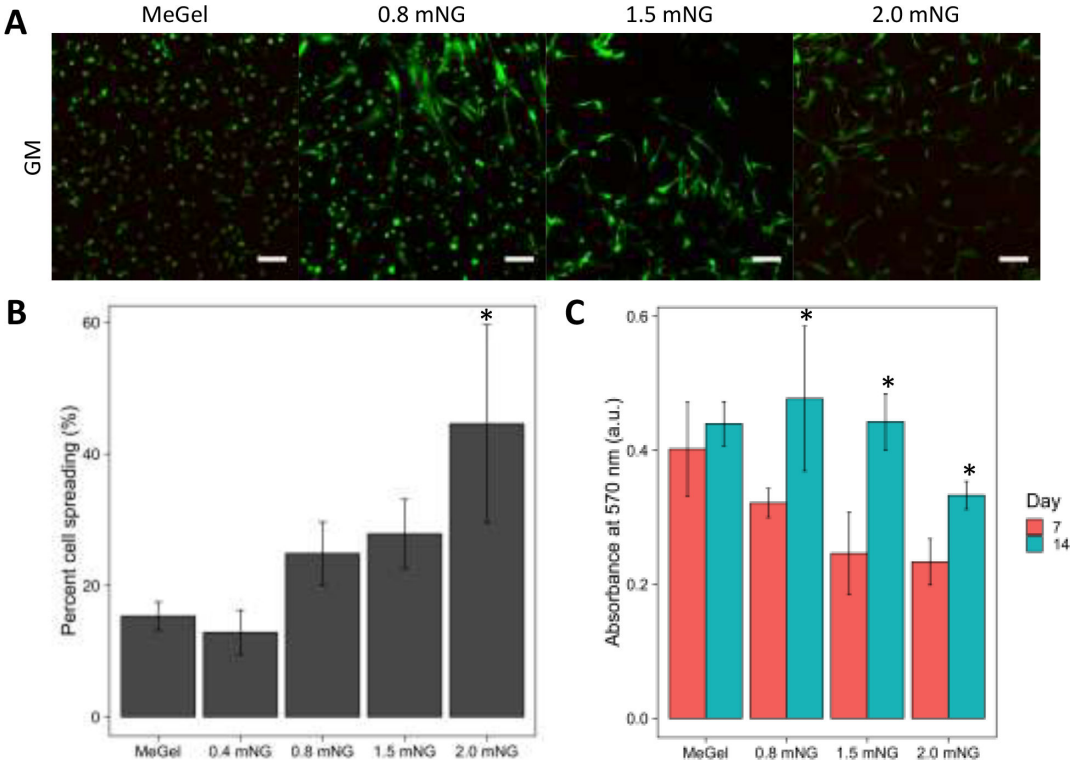

Figure 5.

Biocompatibility of MeGel and mNG hydrogels. (A) Representative images of live/dead staining of cells encapsulated within the different hydrogels(Scale bar = 100 μm); (B) Percent cell spreading in different mNG hydrogels; (C) Cell metabolism over time at D7 and D14 in mNG hydrogels.

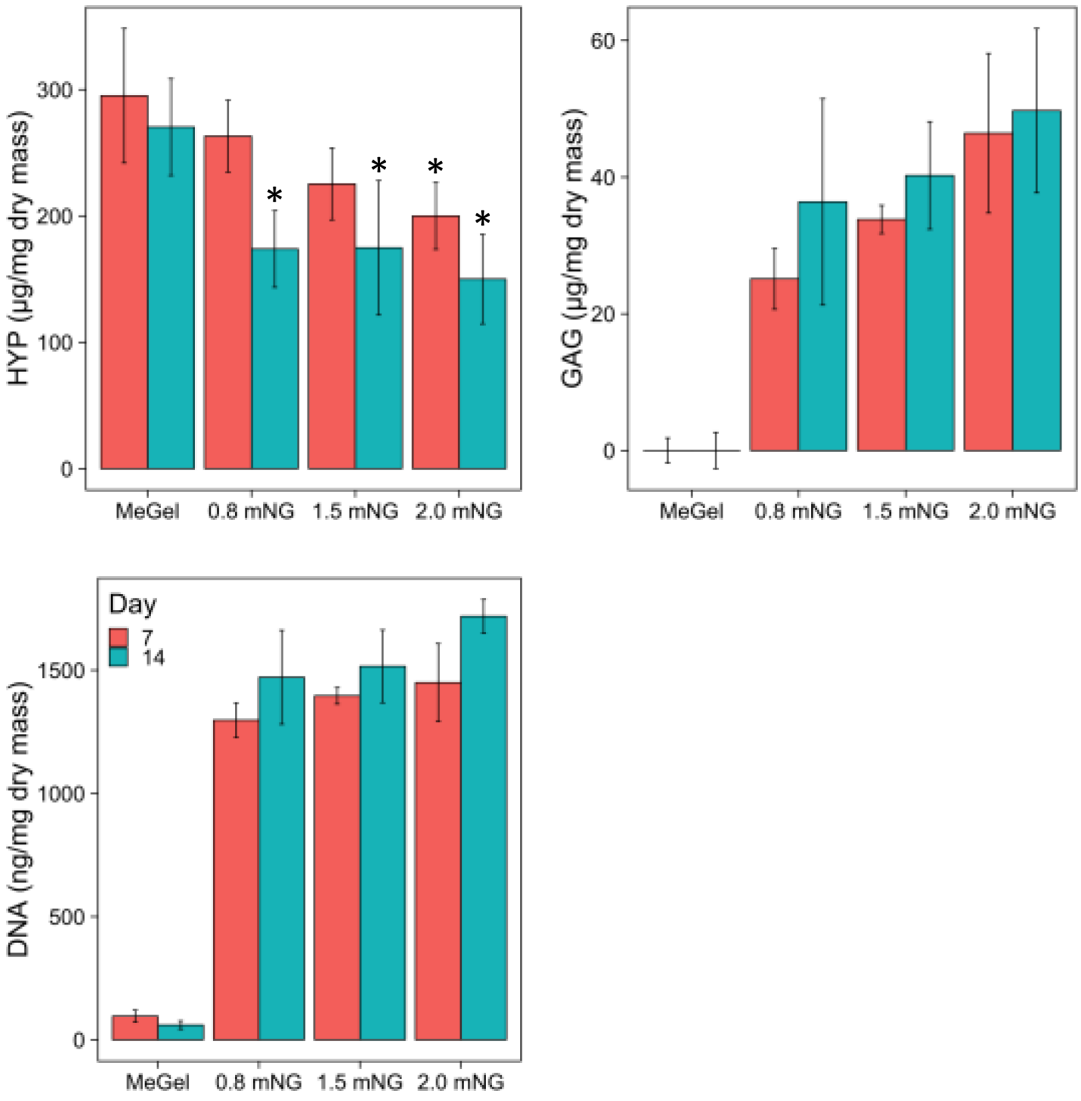

Figure 6.
Quantification of DNA, GAG, and HYP content.

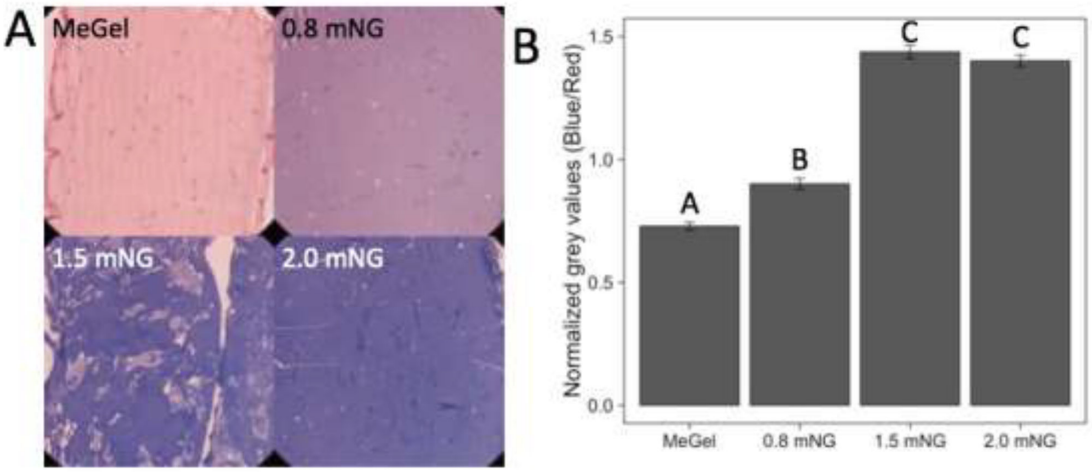

Figure 7.

Alcian blue stain of the different hydrogels at D14. (A) Alcian blue stain on hydrogel sections. (B) Normalized grey values (blue to red).

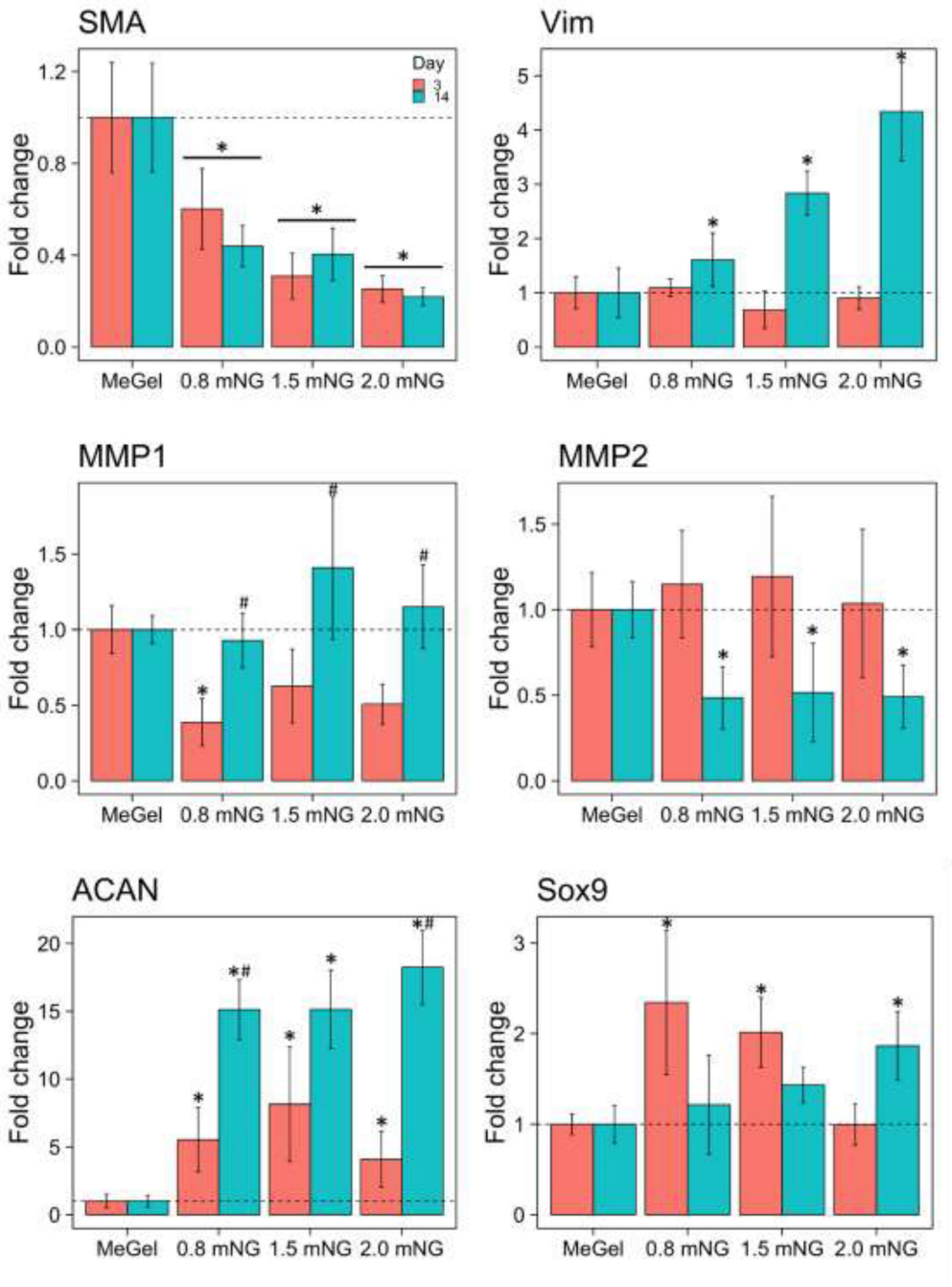

Figure 8.
Gene expression for myofibroblastic (SMA, Vim, MMP1, and MMP2) and chondrogenic/spongiosa (ACAN, Sox9) markers.

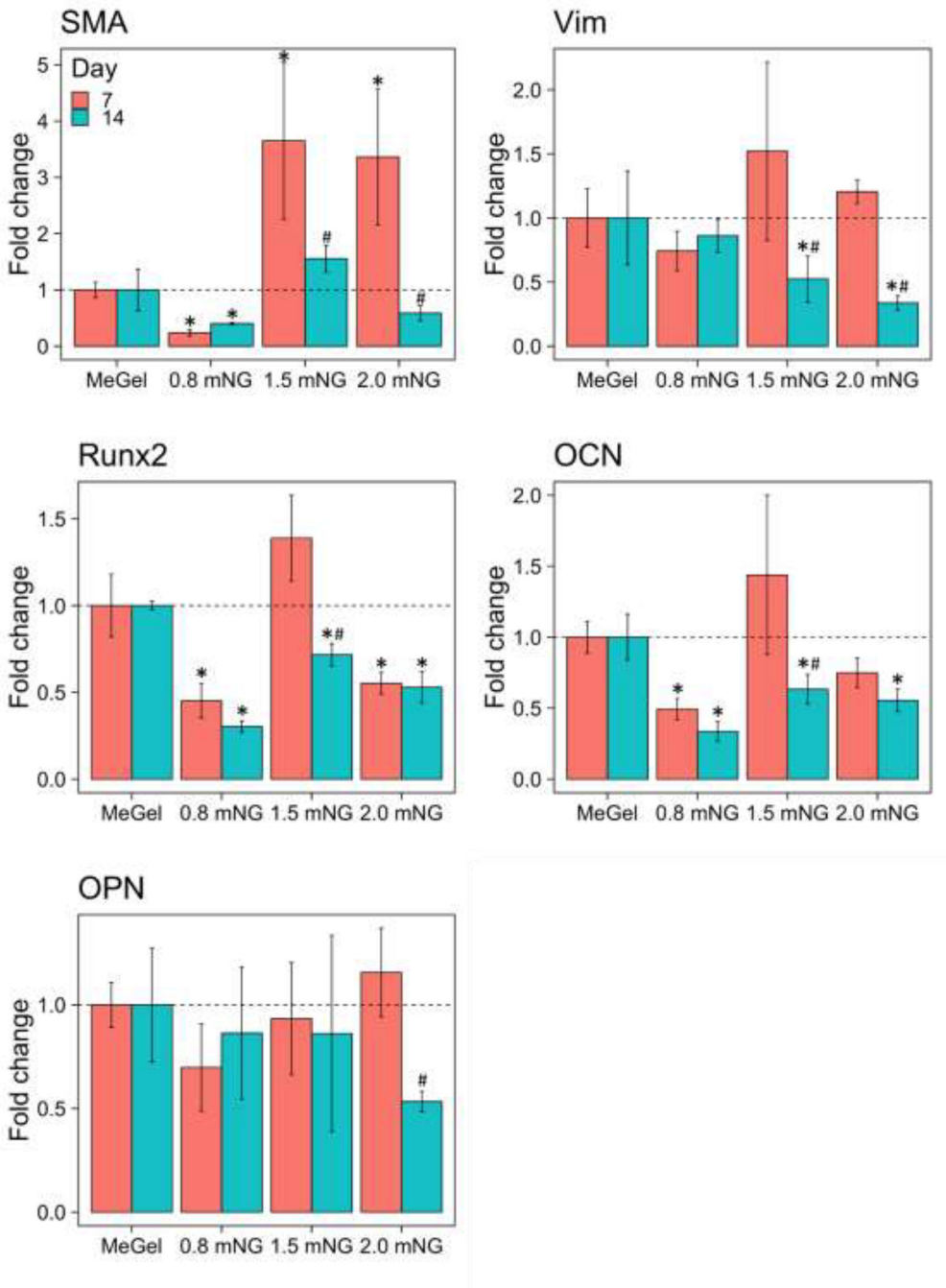

Figure 9.
Gene expression for myofibroblastic (SMA, Vim) and osteogenic (Runx2, OCN, OPN) markers in MeGel and mNG hydrogels in OGM condition.

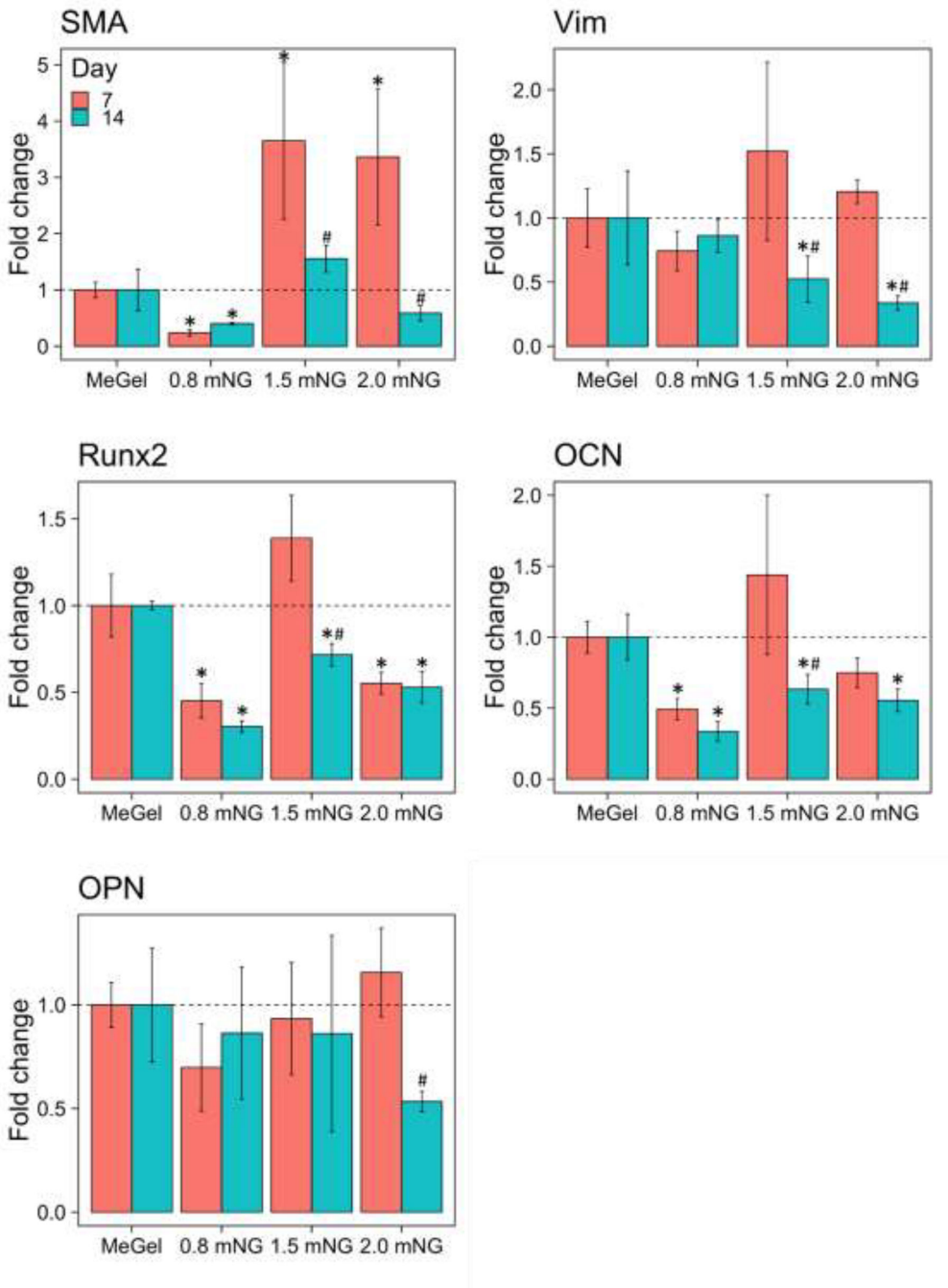

Figure 10.
Comparison of osteogenic genes between GM and OGM conditions at D14.

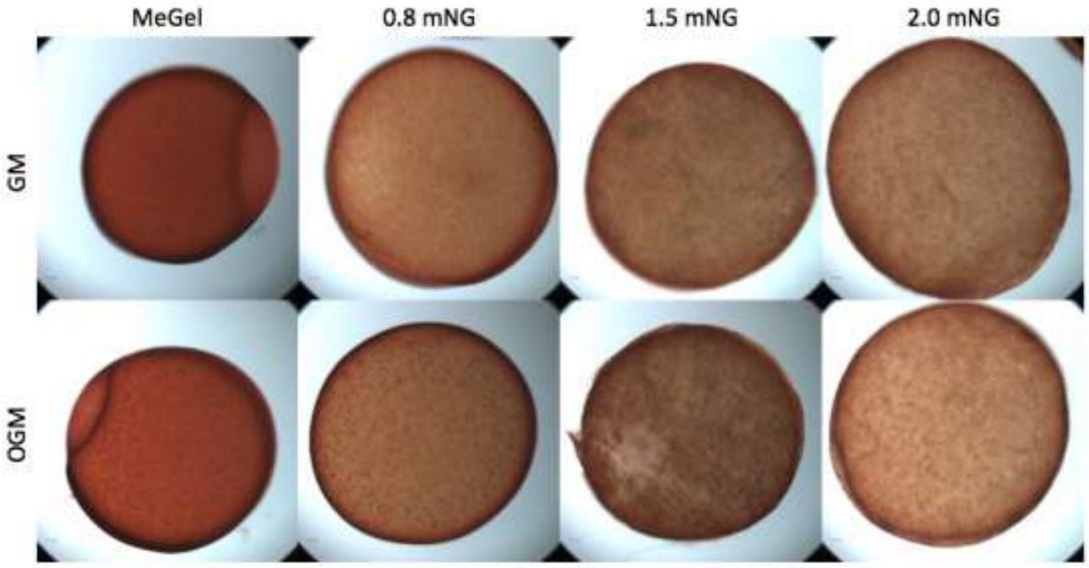

Figure 11.
Alizarin red staining of D14 hydrogels.

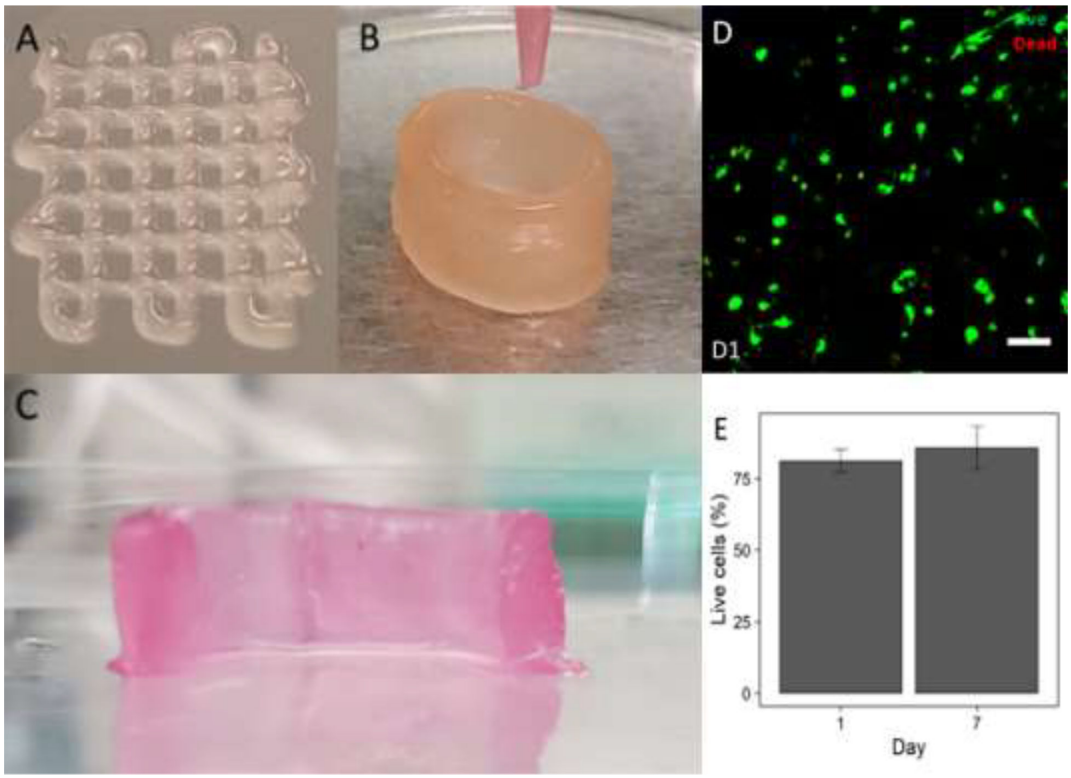

Figure 12.

Bioprinting of mNG hydrogels. (A) a grid pattern and (B) a tubular construct. (C) The cross section of the hydrogel after 7 days in culture. (D) A representative live/dead image show live cells. (E) Quantification of live cells after 7 days.

Table 1.

Components used to conjugate mNCC to MeGel to synthesize mNG

Condition	mNCC	MeGel (g)	6% mNCC (mL)	NHS (mg)	EDC (mg)
0.2 mNG	0.2%	0.7	0.47	6.3	12.5
0.4 mNG	0.4%	0.7	0.93	12.5	25.0
0.8 mNG	0.8%	0.7	1.87	25.0	50.0
1.5 mNG	1.5%	0.7	3.49	46.9	93.8
2.0 mNG	2.0%	0.7	4.65	62.5	125

Table 2.

List of primers used for phenotyping

Gene Symbol	Sequence (5′–>3′)	Ref	Product length (bp)
18S	F: CTTAGTTGGTGGAGCGATTT	NR_003286	170
	R: GCTGAACGCCACTTGTCC		
Vim	F: ACAGGCTTTAGCGAGTTATT	NM_003380	182
	R: GGGCTCCTAGCGGTTTAG		
αSMA	F: CACT GCCGCAT CCT CATC	NM_001613	160
	R: GCTGTTGTAGGTGGTTTCAT		
Runx2	F: CCT CCTACCT GAGCCAGATG	NM_001024630.4	146
	R: CCAGAGGCAGAAGTCAGAGG		
OPN	F: AAATTCTGGGAGGGCTTGG	NM_001040058	117
	R: TTCCTTGGTCGGCGTTTG		
OCN	F: GGCAGCGAGGTAGTGAAGA	NM_199173	148
	R: CCTGAAAGCCGATGTGGT		
Sox9	F: TCCT CAGGCTTT GCGATTT	NM_000346	170
	R: TCCCAGCAGCACCGTTTT		
ACAN	F: GGCGAGT GGAAT GAT GTT	NM_001135	273
	R: CTTCTGTAGTCTGCGTTTGTAG		
MMP1	F: TGAAGAAT GAT GGGAGGCAAGT	NM_002421	122
	R: CAGGGTTTCAGCATCTGGTTTC		
MMP2	F: CCCCAAAACGGACAAAGAG	NM_004530.5	314
	R: CACGAGCAAAGGCATCATCC		